NUMERICAL SIMULATION OF TURBULENT FLOW AND HEAT TRANSFER AROUND A RECTANGULAR PRISM MOUNTED ON THE CHANNEL AXIS IN TANDEM ARRANGEMENT

SAIM Rachid, e-mail: saimrachid@mail.univ-tlemcen.dz
ABBOUDI Said, e-mail: said.abboudi@utbm.fr
FMSTO-ST, UMR CNRS 6174, Département CREST, UTBM, Site de Sévenans- 90100 - France

BENYOUCEF Boumedienne, e-mail: b_benyoucef@mail.univ-tlemcen.dz
Unité de Recherche des Matériaux et Energies Renouvelables (URMER)-Faculté des Sciences –Université Abou Bakr Belkaid-BP 119- Tlemcen-13000- Algérie.

AZZI Ahmed, e-mail: ah_azzi@yahoo.fr
Département de Génie Mécanique, Faculté des Sciences de l'ingénieur –Université Abou Bakr Belkaid-BP 230- Tlemcen-13000- Algérie.

Abstract. *A numerical analysis was carried out to study the turbulent flow and forced convection in a two-dimensional horizontal plane channel containing two rectangular prism mounted on the channel axis in tandem arrangement.The numerical formulation use a finite volume method with power–law scheme and the k-ε model associated with wall function to describe the turbulent flow. The velocity and pressure terms of momentum equation are solved by SIMPLE algorithm. The effects of the dimensionless height of blocks , the dimensionless distance between the blocks Pi on the flow structure and heat transfer characteristics were investigated for the system at various Reynolds number Re and various ratio A/B at Pr =0.71 with constant physical properties. The parameters studied include the entrance Reynolds number Re ($1x10^5$ –$5x10^5$) while varying the blockage ratio of the prism (A= 0.5B, 0.75B and 1.B). Special emphasis is given in the systematic analysis to detail the effect of the Reynolds number (Re_{Dh}). The validity of the numerical simulation presented in the present work has been evaluated by comparing with those of literatture for the same conditions. A quite good agreement is observed between the two studies.*

Keywords*: turbulent flow, Forced convection, obstacle, rectangular channel.*

1. INTRODUCTION

The Flow and heat transfer associated with interrupted surfaces between two parallel walls has been investigated by many researchers both numerically and experimentally. This flow situation is a very important area of research not only because of its academic attractiveness but also owing to the related technical problems associated with energy conservation and structural design. This type of flow is of relevance for many practical applications, such as electronic cooling, turbine blades and heat exchangers systems (H. Abbassi et al. 2001).

The obstacles are used to enhance heat transfer by increasing the heat transfer surface area and by interrupting the wall boundary layer to promote mixing and turbulence (Young and Vafai, 1998) and (Wang and Vafai, 1999).

An extensive experimental studies of turbulent flow past a square bar placed at various distances from an adjacent wall has been performed by (Durao et al. 1991) and (Bosch et al. 1996)

Durao et al. found the critical value for the gap beyond which vortex shedding occurs to be in the range Pi/D=0.25-0.5 bar heights at Re=13600. For Pi/D=0.5 the main contribution to the normal stresses is the vortex shedding, so peaks of the normal stresses are located in the shear layers around the square bar. Bosch et al. at Re=22000 observed steady flow for Pi/D=0.25, while vortex shedding was observed for Pi/D ≥ 0.5.

Bosch and Rodi, (1996) reported calculations with two versions of the k-ε turbulence model for the flow passing a square bar at Re=22000 placed at various distances from an adjacent wall. They obtained the unsteady shedding motion around the bar for Pi/D ≥ 0.5. The predictions of the unsteady velocity vectors for different phases agree well with the experimentally observed mean flow motion (Bosch et al. 1996).

An experimental study was reported by Nakagawa et al. (1999) of heat transfer in a turbulent channel flow with a rectangular bar having various width-to-height ratios, 0.5, 1, 2 and 3, and for three Reynolds numbers. Time-averaged heat transfer coefficients on the heated channel wall have been measured. They measured heat flux fluctuation with thin-film heat flux sensors in three points of the channel wall, and they used the smoke wire method for flow visualization. They conclude that the wall heat flux fluctuates in phase with the shedding vortices from the bar. The position of the maximum wall heat flux moves downstream as the shedding vortices travel through the channel, which results in extensive heat transfer enhancement.

Numerically, investigations have been performed in two and tree dimensions with turbulent flows. Simulation by vortex shedding over a square cylinder was carried out by Bosch and Rodi (1998). They indicated that the *k-ε* turbulence model predicted flow properties within reasonable accuracy, and Kato Launder modification improved the

predictions considerably. Fully developed channel flows have been extensively studied, and the experiments of Drain and Martin (1985) and Liou et al. (1993) have been frequently used for turbulence model validation.

Drain and Martin performed laser-Doppler velocimetry measurements of the velocity field of water flow in a channel with one wall roughened by periodic ribs.

Liou et al. conducted the corresponding heat transfer measurements for the same geometry in an airflow using the holographic inters geometry technique. The most recent numerical studies on these two cases include Bredberg and Davidson, (1999) and Tsai et al. (2000), Hsieh et al. (2005)

Other numerical study was performed by Valencia (2000) to compute the heat transfer and friction in a channel with a mounted square bar of different sizes detached from the channel wall. The influence of the Reynolds number and the size of the obstacle are examined. The channel walls are subjected to a constant wall temperature. For the simulations, the standard k-ε turbulence model and a modified version proposed by Launder and Kato (1993) were used in conjunction with the Reynolds-averaged momentum and energy equations, and compared thereafter. For the evaluation of the performance of the used numerical methods and the k-ε turbulence model, the experimental results of Nakagawa et al. (1999) of the local Nusselt numbers were used. The comparison of time averaged local Nusselt numbers distribution on the heated channel wall shows that the simulated heat transfer coefficients agree well with the experimental results except in the recirculation zone behind the bar. The differences can be explained by the inadequate experimental position of the bar for the simulation. Valencia compared the computed local heat transfer coefficient between the standard k-ε turbulence model and the modified version of the standard k-ε turbulence model proposed by Launder and Kato (1993), the differences among the Nusselt numbers calculated with LK model and standard k-ε model were small. Alvarez and Valencia (2000) also showed that the displacement of the bar from the channel axis toward the wall did not cause an increase in the global heat transfer coefficient on the channel walls compared with one bar centred in the channel.

The purpose of the present study is to investigate a turbulent fluid flow and heat transfer in a plane channel with two in-line mounted rectangular bars in the thermal entrance region and in the fully developed region with the bars repeated in a spatially periodic fashion. The objectives of the present work are to study the fluid flow and heat transfer in a channel with periodically mounted transverse vortex generators, and we want to quantify also the differences on mean Nusselt number and friction factor calculated with periodic boundary conditions (PBC) compared with the corresponding calculated after the fifth row.

2. PROBLEM STATEMENT AND GOVERNING EQUATIONS

2.1. Statement of the problem

The geometry of the problem is shown in Fig. 1, Consider the steady, incompressible two-dimensional flow of a power law fluid past a rectangle obstacle placed symmetrically in a channel (height D). Furthermore, the thermophysical properties of the fluid are assumed to be independent of temperature.
Where the obstacle pitch to obstacle height ratio is L/D=5 and the channel height-to-obstacle height ratio is B/D=0.152. The measurements of Alvarez, J et al (2000) were conducted at a Reynolds number based on the bulk mean velocity and hydraulic diameter (twice the channel height) of 10^5 for the flow fields and the thermal field. In this study the channel top wall and the bottom wall was heated by a constant temperature T_w=100°C

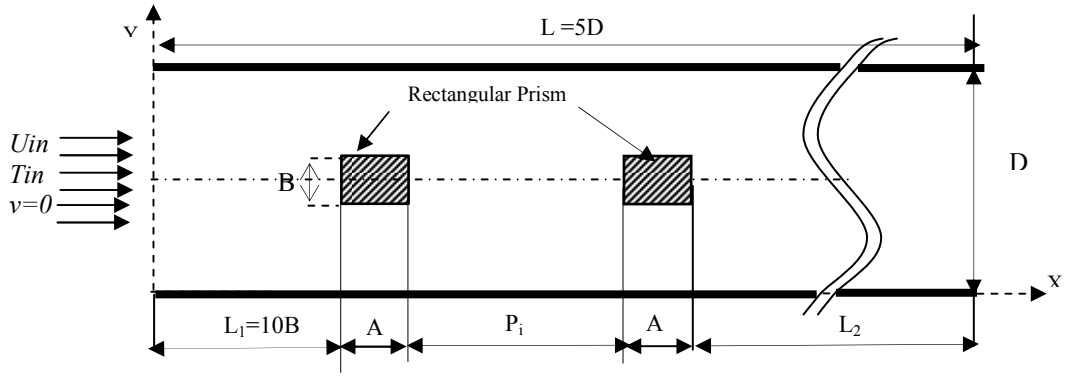

Figure 1. Geometry of the physical problem and boundary conditions

2.2. Governing Equations

Under these conditions, the equations of continuity, momentum and thermal energy (in the absence of viscous dissipation) for a power law fluid in their dimensionless form are written, in Cartesian tensor notation, as

$$\frac{\partial}{\partial x_j}\left(u_j\right)=0 \tag{1}$$

$$\frac{\partial}{\partial x_j}\left(u_j u_i\right) = -\frac{1}{\rho}\frac{\partial P}{\partial x_i} + \frac{\partial}{\partial x_j}\left[\nu\left(\frac{\partial u_i}{\partial x_j} + \frac{\partial u_j}{\partial x_i}\right) - \overline{u_i' u_j'}\right] \tag{2}$$

$$\frac{\partial}{\partial x_j}\left(u_j T\right) = \frac{\partial}{\partial x_j}\left[\alpha\left(\frac{\partial T}{\partial x_j} - \overline{u_j' T'}\right)\right] \tag{3}$$

Where: u_j is the time-averaged velocity in the x_j-direction, with j =1 or 2 representing. The streamwise x or vertical y direction; $(x_1, x_2) \equiv (x, y)$ and $(u_1, u_2) \equiv (u, v)$

ρ is the density of the air, ν is the kinematic viscosity, α is the thermal diffusivity, $\overline{u_i' u_j'}$ is the Reynolds stress and $\overline{u_j' T'}$ is the turbulent heat flux

2.3 Turbulence models

In the two-equation k-ε models, the Reynolds stresses $\left(\overline{u_i' u_j'}\right)$ and turbulent heat fluxes $\left(\overline{u_j' T'}\right)$ are modelled in terms of the eddy viscosity (ν_t), turbulent kinetic energy (k) and its dissipation rate (ε). Based on series-expansion arguments by Pope (1975), the stress-strain relationship can be written as:

$$\frac{\overline{u_i' u_j'}}{k} = \frac{2}{3}\delta_{ij} - \underbrace{\frac{\nu_t}{k} S_{ij}}_{linear\ \ term} + \underbrace{c_1 \frac{\nu_t}{\varepsilon}\left(S_{ik}S_{kj} - \frac{1}{3}\delta_{ij}S_{kl}S_{kl}\right) + c_2 \frac{\nu_t}{\varepsilon}\left(\Omega_{ik}S_{kj} - \Omega_{jk}S_{ki}\right) + c_3 \frac{\nu_t}{\varepsilon}\left(\Omega_{ik}\Omega_{jk} - \delta_{ij}\Omega_{kl}\Omega_{kl}\right) + HOT}_{Quadraticterm} \tag{4}$$

Where HOT denotes higher order terms, for HRN (*High-Reynolds Number)* k-ε models

$$\nu_t = c_\mu \frac{k^2}{\varepsilon} \tag{5}$$

$$S_{ij} = \frac{\partial u_i}{\partial x_j} + \frac{\partial u_j}{\partial x_i} \tag{6}$$

$$\Omega_{ij} = \frac{\partial u_i}{\partial x_j} - \frac{\partial u_j}{\partial x_i} \tag{7}$$

The turbulent heat fluxes are modelled using the Boussinesq approximation as

$$\overline{u_j' T'} = -\frac{\nu_t \partial T}{Pr_t \partial x_j} \tag{8}$$

Where $Pr_t = 0.9$ is the turbulent Prandtl number used in wall-bounded flows.

2.4. High-Reynolds Number k-ε model with wall functions:

The governing equations for the HRN k- ε model are written as

$$\frac{\partial}{\partial x_j}\left(u_j k\right) = \frac{\partial}{\partial x_j}\left(\frac{\nu_t}{\sigma_k}\frac{\partial k}{\partial x_j}\right) + P_k - \varepsilon \tag{9}$$

$$\frac{\partial}{\partial x_j}\left(u_j \varepsilon\right) = \frac{\partial}{\partial x_j}\left(\frac{\nu_t}{\sigma_\varepsilon}\frac{\partial \varepsilon}{\partial x_j}\right) + \frac{\varepsilon}{k}\left(C_{\varepsilon 1} P_k - C_{\varepsilon 2}\varepsilon\right) \tag{10}$$

Where σ_k=1.0, σ_ε =1.3, $C_{\varepsilon 1}$=1.44 and $C_{\varepsilon 2}$=1.92 are model constants recommended by Launder and Spalding (1974). The turbulence production term (P_k) in the k-equation is defined as:

$$P_k = -\overline{u_i' u_j'}\frac{\partial u_i}{\partial x_j} \tag{11}$$

2.5. Near Wall Treatment

Wall functions given by Launder and Spalding (1974) are employed to prescribe the boundary condition along the faces of the faces of the two obstacles and the channel walls of the computational domain. The wall functions are based on the logarithmic law of the wall, assume that the near-wall region consists of two layers: the inner layer which

extends from the wall up to $y^+ = 11.63$, and the outer layer where $y^+ \rangle 11.63$. The dimensionless wall-normal distance is given by:

$$y^+ = yu_\tau / \nu \tag{12}$$

or

$$y^+ = \frac{\rho y_p C_\mu^{1/4} K_p^{1/2}}{\mu} \tag{13}$$

Where $u_\tau = \sqrt{\tau_w / \rho}$ the friction velocity and τw is the wall shear stress defined as:

$$\tau_w = \frac{\rho U_p C_\mu^{1/4} K_p^{1/2} \kappa}{ln\left(Ey^+\right)} \tag{14}$$

where $\kappa = 0.42$ is the von Karman constant and E =9.8 is an integration constant for smooth walls.
The production rate of k and the averaged dissipation rates over the near-wall cell for the k-equation as well as the value of ε at the point p are computed respectively from the following equation:

$$p_k = \tau_w \frac{U_p}{y_p} \tag{15}$$

$$\bar{\varepsilon} = \frac{C_\mu^{3/4} K_p^{3/2}}{\kappa y_p} ln\left(Ey^+\right) \tag{16}$$

$$\varepsilon_p = \frac{C_\mu^{3/4} K_p^{3/2}}{\kappa y_p} \tag{17}$$

For the temperature boundary condition, the heat flux to one channel wall is derived from the thermal wall function:

$$q_w = \frac{\left(T_w - T_p\right)\rho C_p C_\mu^{1/4} K_p^{1/2}}{Pr_t\left(ln\left(Ey^+\right)/\kappa + PP\right)} \tag{18}$$

where the empirical function PP is specified as:

$$PP = \frac{\pi/4}{sin\left(\pi/4\right)}\left(\frac{A}{\kappa}\right)^{1/2}\left(\frac{Pr}{Pr_t} - 1\right)\left(\frac{Pr_t}{Pr}\right)^{1/4} \tag{19}$$

Local Nusselt numbers on the channel walls were computed with the following equation:

$$Nu(x) = \frac{h(x)D}{K} = \frac{q_w D}{K\left(T_w - T_b(x)\right)} \tag{20}$$

Considering that the computation is confined in one cycle and the difference between wall temperature T_w and bulk temperature $T_b(x)$.

$$T_b(x) = \frac{\int_A u(x,y) \cdot T(x,y)\, dA}{\int_A u(x,y) \cdot dA} \tag{21}$$

2.6. Boundary Conditions

The computational domain and boundaries are shown in Fig. 1. The problem analysed is to be turbulent flow in rectangular channel with rectangle blocks placed symmetrically in a channel. The boundary conditions for the above set of governing equations are:

(1) Inlet boundary (1-2)

$u = U_{in}$, $v = 0$, $T = T_{in}$ (22)

$$k_{in} = 0.005\ U_{in}^2 \tag{23}$$

$$\varepsilon_{in} = 0.1 k_{in}^{3/2} \tag{24}$$

Where k_{in} is the inlet condition for the turbulent kinetic energy and ε_{in} is the inlet condition for the dissipation rate.

(2) Wall sides

- The no-slip condition is assumed: $u = v = 0$.
- In the *k*-ε model, the near-wall region was simulated by wall function suggested by Launders and Spalding (1974).
- For the kinetic energy, at the upper and lower walls we supposed:

$$\left.\frac{\partial k}{\partial n}\right|_w = 0 \tag{25}$$

Where n is the normal coordinate to the wall,
ε is computed in the adjacent volume P to the wall as:

$$\varepsilon_p = \frac{C_\mu^{3/4}.k_p^{3/2}}{\kappa.y_p} \tag{26}$$

(3) Exit boundary (3-4)
At the outlet, all gradients are assumed to be zero:

$$\begin{aligned} &\partial u/\partial y = 0 \\ &\partial v/\partial y = 0 \\ &\partial T/\partial y = 0 \end{aligned} \tag{27}$$

(4) Interfacial boundary: at the solid-fluid interface, the following condition is applied:

$$\lambda_f \frac{\partial T_f}{\partial x} = \lambda_s \frac{\partial T_s}{\partial x} \quad \text{and} \quad T_f = T_s \tag{28}$$

(5) All the walls are maintained at a constant temperature T_w.

3. NUMERICAL DETAILS

A computer code based on the finite volume technique is developped to solve the governing equations describing the flow and heat transfer in this problem. The SIMPLE algorithm (Semi-Implicit Method for Pressure-Linked Equations) was adopted. The diffusion terms appearing in the transport equations for momentum and turbulence parameters are discretized using second-order central differencing. The Power-Law Differencing Scheme (PLDS) of Patankar (1980) were used to approximate the convection terms. The discretized governing equation is typically solved using the Tri-Diagonal Matrix Algorithm (TDMA).

3.1. Convergence Criteria

The convergence of the iterative algorithm is ensured when the normalized velocity and mass residuals are less than a prescribed value. The iterative solution is continued until the residuals, for all computational cells, became less than 5.10^{-4}, for all dependent variables. This value corresponds to a reduction in the residuals of approximately four orders-of-magnitude from the start to the end of the calculation. It was verified that using more stringent convergence criteria, had no effect on the results. The non uniform grid in x and y directions were found to model accurately the fluid flow and heat transfer in this problem. This grid is highly concentrated close to the block to capture high gradient velocity, pressure and temperature. In order to ensure grid independence of the results, a series of tests for non uniform grids were carried out. The choice of the grid distribution (300× 120) is found to be sufficient for the range of Reynolds numbers investigated.

4. RESULTS AND DISCUSSION

4.1. Validation

In order to demonstrate the validity and precision of the model and the computer code, calculated velocity profiles have been compared with corresponding experimental results from the literature. Fig. 2 compares the results of the present work with those of Alvarez, J et al (2000) for the same conditions. We present the mean Nusselt number on the channel wall for fully developed turbulent. A quite good agreement is observed between the two studies.

4.2. Velocity vector plots

Figure 3 shows a velocity vectors plot of the overall computational domain along x-axis. The flow around rectangular cylinder at the steady state under Re=10000, A=0.152D, B=0.304D and P_i= 5.5d.
The recirculating zone is generated at downstream from the prism, and the reattachment regions are clearly seen. Also, another recirculation is generated at the upstream from the obstacle. The flow separates from the leading edges of rectangular cylinder and large recirculation zones are observed behind the first and the second rectangular cylinder. The distributions of the iso velocity lines are denser near the front surface of the rectangular cylinder than those of the other surfaces of rectangular cylinder. Another unique feature of the flow field consists of the presence of counters-clockwise (region below rectangular cylinder) and clockwise (region above rectangular cylinder). A third and more important zone of the perturbation of the flow is also generated between the first and the second rectangular cylinder. In the numerical results, Fig. 4 shows the mean velocity profiles for the position x=2.24, x=8.06 and x=9.55, calculated downstream of the entrance and their position are located of the first rectangular cylinder.

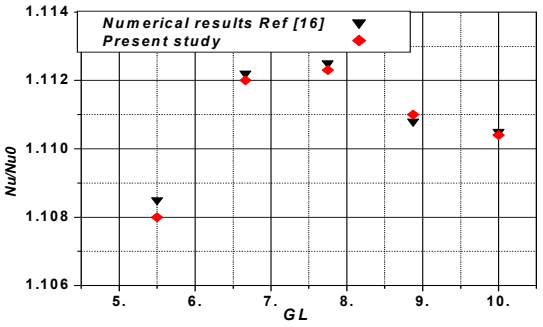

Fig 2. Comparison of present study with that of Alvarez, J et al (2000)

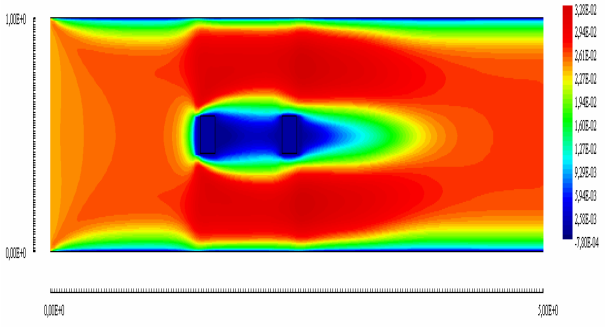

Fig 3. Velocity of the flow in the symmetry plane of the 2D obstacles.

The influence of deformation of the flow field increases as the flow approaches the first rectangular cylinder, increasing the velocity of the flow approaching the passage under the rectangular cylinder. The representation of the dimensionless velocity profiles just upstream of the first rectangular cylinder is shown in Fig. 5 for Re=1.E+5, B/D=0.152, B=2A and Pi=5.5d. It is observed that clockwise of flow becomes more in more intense behind the rectangular cylinder (x=9.22, 9.39, 9.55). Fig. 6 shows the dimensionless velocity profiles between the first and the second block at Re=1.E+5, B/D=0.152 and B=2A. Their locations are by x=11.5, x=12.7 and x=15 from the entrance, i.e. 4, 2.8 and 0.5 before the second rectangular cylinder. The flow is characterized by the very high velocities at the lower and the upper part of the channel, approaching 300 % of the reference velocity. Negative velocities indicate the presence of the recirculation zone behind the first and the second block.

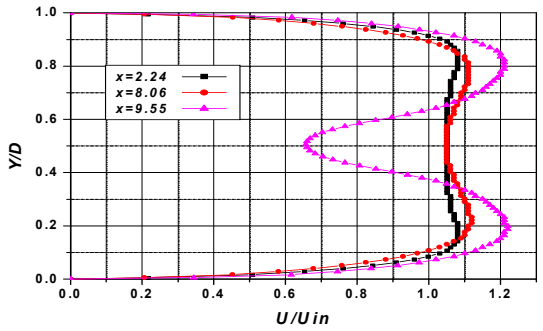

Figure 4. Dimensionless velocity profiles upstream of the first rectangular cylinder for Re=1.E+5 , for Re=1.E+5, B/D=0.152 and B=2A

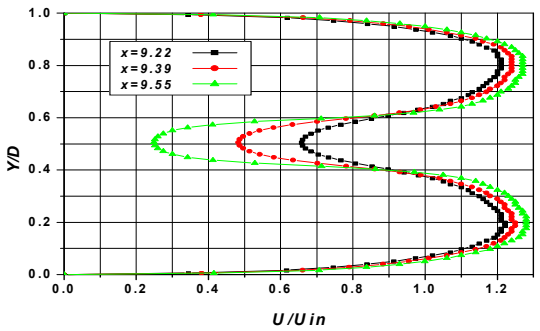

Figure 5. Dimensionless velocity profiles just upstream of the first rectangular cylinder for Re=1.E+5, B/D=0.152 and B=2A

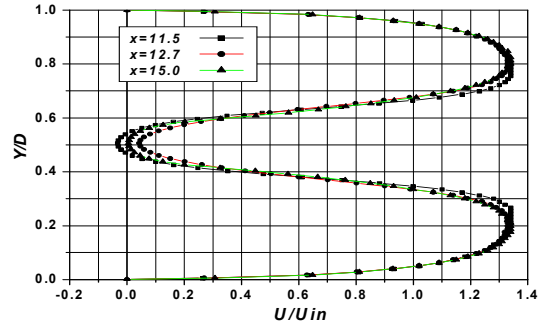

Figure 6. Dimensionless velocity profiles between the first and the second rectangular cylinder for Re=1.E+5 , B/D=0.152 and B=2A

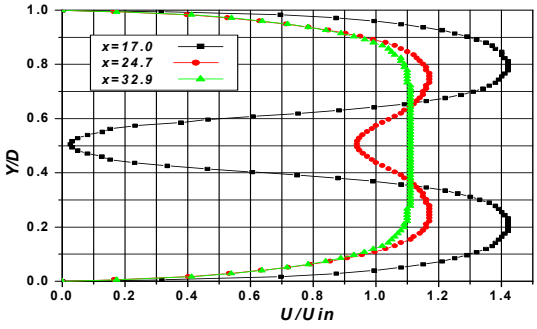

Figure 7. Dimensionless velocity profiles downstream of the second rectangular cylinder for Re=1.E+5 , B/D=0.152 and B=2A

4.3. Temperature field

Figure 8 shows the temperature field distribution in the symmetry plane of he 2D rectangular cylinder at Re=1.E+5, B/D=0.152 and B=2A. Numerical results show very low temperature values adjacent to the prism. In the region downstream of both rectangular cylinders, recirculation cells with very low temperature are observed. In the regions between the tip of the obstacle and the channel wall, the temperature is increased. Due to the changes in the flow direction produced by the block, the highest temperature values appear behind the lower channel wall with acceleration process that starts just after the second rectangular cylinder.

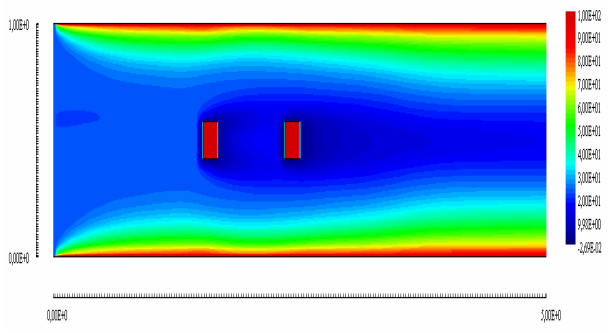

Figure 8. Dimensionless temperature distribution in the symmetry plane of the 2D rectangular cylinder for Re=1.E+5, B/D=0.152 and B=2A

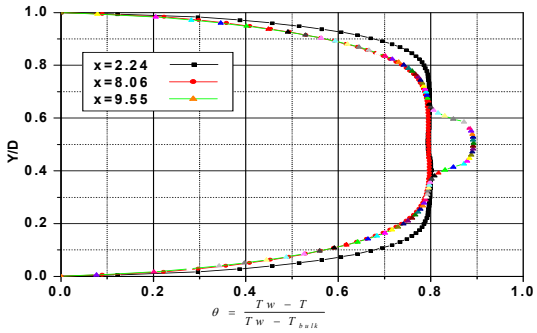

Figure 9. Dimensionless Temperature profiles upstream of the first rectangular cylinder for Re=1.E+5, B/D=0.152 and B=2A

The dimensionless temperature profiles are plotted in Fig. 9 as a function the channel distance at Re=1.E+5, B/D=0.152 and B=2A. This Figure, clearly shows that the temperature gradient at the heated wall decreases (i.e., the heat transfer rate from the heated wall decreases) with increasing the flow velocity. This is because the introduction negative velocity on the turbulent forced-convection flow reduces the level of turbulence intensity inside the boundary layer. The recirculating region and the temperature lines are both restricted to the lower and the upper corner of the first rectangular cylinder. The cold external air flows parallel along the top and bottom walls. As the flow progresses, the amounts of the recirculating zone increase between the first and the second obstacle.

4.4. Effect of Reynolds number

The effects of Re on flow pattern and temperature field for the case of B/D=0.152 and B=2A and λ_s/λ_f =100 are shown in Fig. 10. Moreover, this figure represents the local Nusselt number obtained for each of the two rectangular cylinders but for values of the Reynolds number equal to 1.E+5, 2.5E+5 and 5.E+5. As expected, it can be clearly observed that values of the Nusselt number become higher with increasing values in the Reynolds number. For the height value of Reynolds number (Re=5.E+5), the Nusselt number for the first rectangular cylinder is greater than that of the second. At low Reynolds number values, the Nusselt number for the second obstacle becomes nearly equal to that the first one.

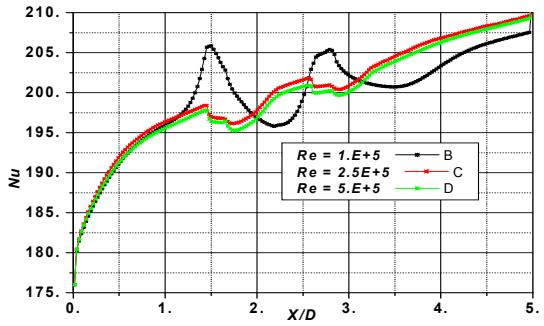

Figure 10. Effect of Reynolds number on the local Nusselt number for B/D=0.152 and B=2A: (1) Re=1.E+5, (2) Re=2.5E+5, (3) Re=5.E+5

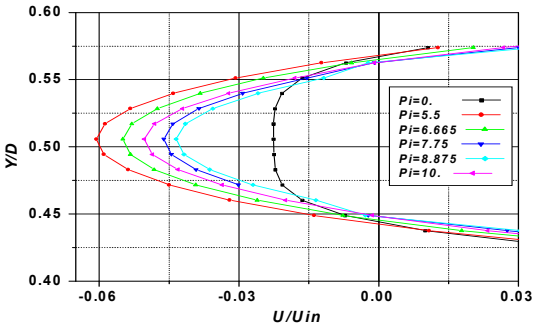

Figure 11. Effects of the Pitch Pi on recirculation zone just downstream the first obstacle: Re=1.E+5, (a) Pi=0. ,(b) Pi=5.5, (c) Pi=6.665, (d) Pi=7.75, (e) Pi=8.875, (f) Pi=10.

4.5. Effect of the pith length

In this section, the structure of turbulent flow in the channel with square bars (A=B) mounted in the channel axis in tandem arrangement calculated with k-ε model will be discussed. Fig. 12 shows maps of fluctuating velocity vector for four tandem arrangements Pi=5.5, 6.665, 7.75, 8.875 and 10.

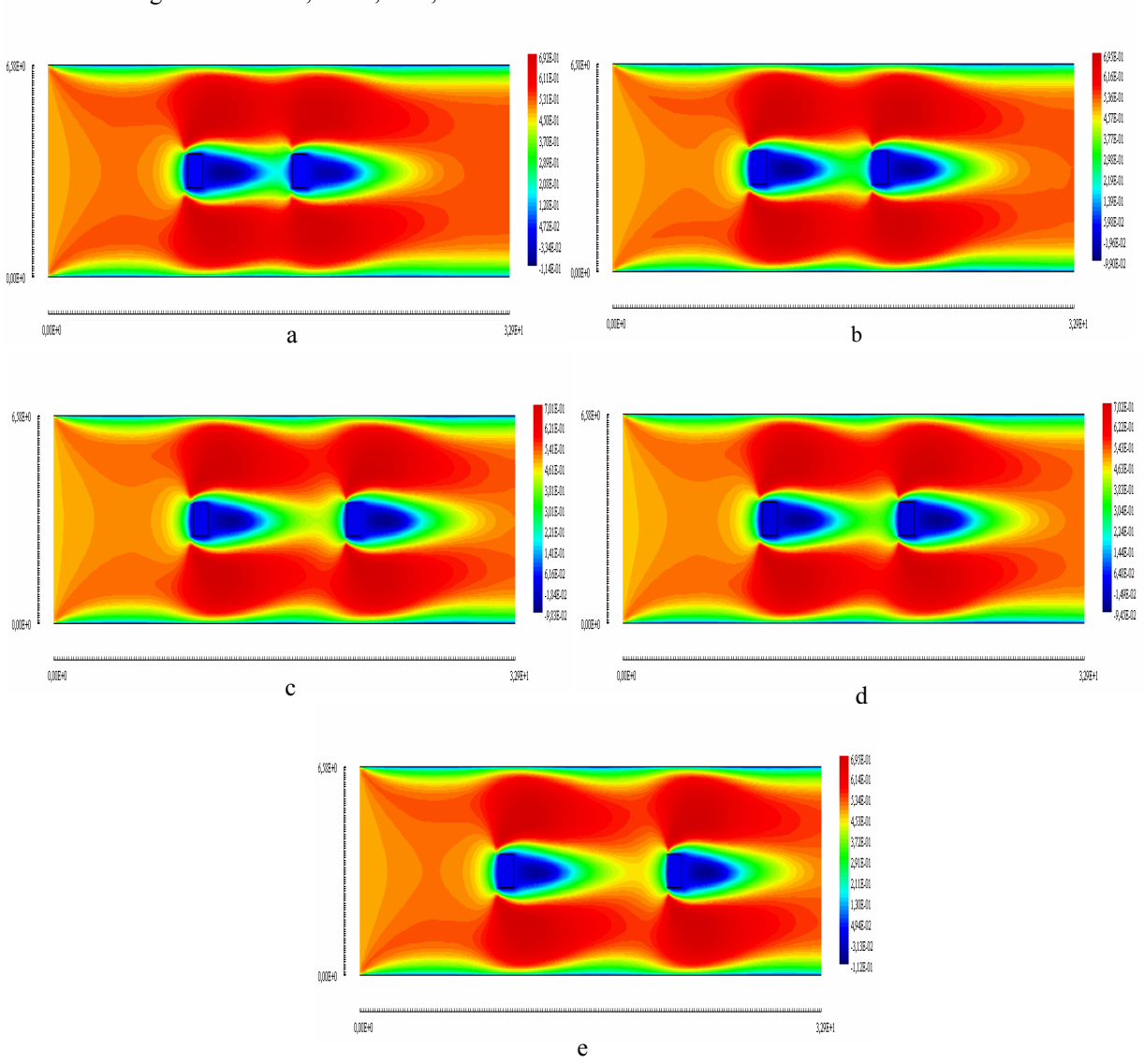

Figure 12. Contours of velocity vectors for tandem arrangements: (A=B), Re=1.E+5, (a) Pi=5.5, (b) Pi=5.5, (c) Pi=6.665, (d) Pi=7.75, (e) Pi=10.

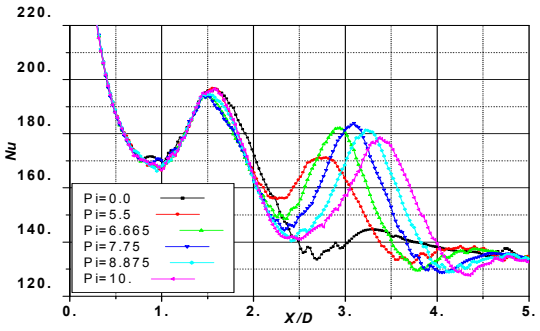

Figure 13. Effects of the Pitch Pi on local Nusselt number for A=B and Re=1.E+5 (a) Pi=0. ,(b) Pi=5.5, (c) Pi=6.665, (d) Pi=7.75, (e) Pi=8.875, (f) Pi=10.

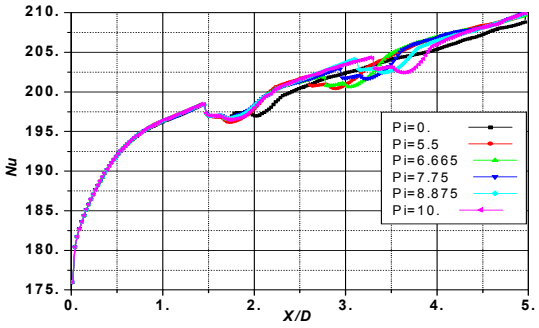

Figure 14. Effects of the Pitch Pi on mean Nusselt number for A=B and Re=1.E+5 (a) Pi=0. ,(b) Pi=5.5, (c) Pi=6.665, (d) Pi=7.75, (e) Pi=8.875, (f) Pi=10.

In this study it is observed that the effects of the of pitch length on the velocity profile just downstream the first bars (x=12.7) are will be focused our attention. The results indicate that the sizes of the recirculation regions over the first square cylinder are more important as the arrangement increases. The recirculating region changes its orientation behind the first bar. The velocity is highly affected by the pitch arrangement Pi. Fig 12 illustrates the recirculation zone downstream the first obstacle for the various Pi considered in this study.

Finally, the effect of pitch length is shown in Fig. 13 and 14 where de Nusselt number increases over the rectangular cylinder wall by increasing Pi. This result is consistent with the presence of vortices at these boundaries. The heat transfer is characterised by the value of the Nusselt number obtained for values of longitudinal spacing between bar's centers pi=5.5, 6.665, 7.5, 8.885 and 10. Moreover, the obstacle spacing seems to have significant effects on the distribution of the local Nusselt number in the channel.

4.6. Effect of the blockage ratio

The effect of the blockage ratio (A/B) on the Nusselt number for the solid- type rectangular cylinder is shown in fig. 15 and fig. 16. The result indicate that the Nusselt number increases with increasing A/B because the cross-sectional area where the flow passes through gets smaller for a fixed rectangular cylinder spacing and a given Reynolds number. It further found that at the same rectangular cylinder blockage (A/B=1) the Nusselt number Coming to the effects of blockage of the rectangular cylinder on the rate of heat transfer, Fig. 14 illustrates the influence of the rapport A/B. The Nusselt number of the upper wall of the channel decreases with increasing blockage ratio. This behaviour can be explained by the increasing size and strength of the primary vortex behind the rectangular cylinder and the quick disappearance of the secondary vortex at the lower wall. Again, this vortex reduces heat transfer from the wall of the channel and from the wall of the rectangular cylinder to the fluid.

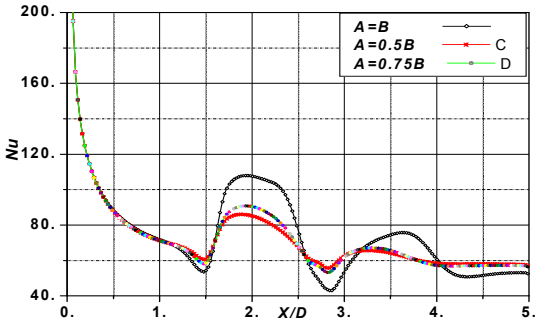

Figure 15. Effect of blockage ratio (A/B) on the local Nusselt number for Re=1.E+5 (B) A/B=1, (C) A/B=0.5 , (D) A/B=0.75

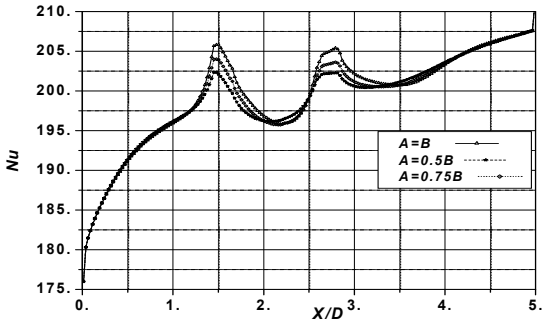

Figure 16. Effect of blockage ratio (A/B) on the local Nusselt number for Re=1.E+5 , (1) A/B=1, (2) A/B=0.5 , (3) A/B=0.75

5. CONCLUSION

The turbulent flow and heat transfer in horizontal channel containing two rectangular cylinders located symmetrically in tandem along the channel axis. The geometry of the problem is a simplification of the geometry found in many industrial applications. A numerical simulation has been systematically performed for the flow with the standard k-ε turbulence model. The SIMPLE_HT computer code was modified and tested for validity. A comparison of velocity profiles with a numerical investigation of the same problem in a channel with two mounted square bars showed similar Nusselt number distribution. The results are presented for a fixed bar spacing (Pi=5.5A) and different values of Reynolds number ($1x10^5 \le Re \le 5x10^5$), blockage ratio (A/B=0.5, 0.75 and 1).

Conclusions can be summarized as follows:

(1) There are three effects present when the solid-type rectangular cylinder is presented in fluid flow, increasing of heat transfer and changing the flow transport phenomena.

(2) The flow and heat transfer numerical calculations present that the different transport phenomena around the solid type prism exists behind the solid.

(3) The numerical results show that the present numerical model in the tandem arrangements the downstream prisms intensifies the detachment of vortices and therefore the local heat transfer increases strongly after the second baffle.

(4)Reynolds number has the effect of expanding the primary vortex over the wall of the two baffles. A distortion of the temperature distribution near the end of the flow field has been observed to occur as Reynolds number increase. This behaviour is believed to be caused by the presence of the second prism that distorts both the flow and temperature fields.

(5) As the blockage ratio is increased, the vortex behind the baffle grows rapidly and causes the rate of heat transfers.

(6) Changing the spacing between obstacles seemed to reduce to changing the heat transfer and fluid flow in the sense that higher heat transfer is obtained for higher bar spacing
(7) A comparison of the present prediction shows good agreement with numerical study of Alvarez, et al. (2000). The Deviation can be found near the recirculating bubble behind the rectangular cylinder.

6. REFERENCES

Abbassi, H., Turki, S., Nasrallah, S. B., 2001, "Numerical investigation of forced convection in a plane channel with a built-in triangular prism", International Journal Thermal. Vol. 40, pp. 649–658

Alvarez, J. , Pap. M and Valencia, A, 2000, "Turbulent heat transfer in a channel with bars in tandem and in side by side arrangements", International Journal of Numerical Methods for Heat & Fluid Flow, Vol. 10 No. 8, pp. 877-895.

Bengt Sundén,M. Rokni, M. Fghri and Daniel Eriksson, 2004 "SIMPLE_HT, The computer code simple_ht for computational heat transfer", (Department of heat and power engineering- Division of heat transfer- Lund Institute of Technology)

Bosch, G., Kappler, M. and Rodi, W. 1996, "Experiments on the flow past a square cylinder placed near a wall", Experimental Thermal and Fluid Science, Vol. 13, pp. 292-305.

Bosch, G. and Rodi, W. 1996, "Simulation of vortex shedding past a square cylinder near a wall", International Journal of Heat and Fluid Flow, Vol. 17, pp. 267-75.

Bosch. G and Rodi. W, 1998, "Simulation of Vortex Shedding Past a Square Cylinder with Different Turbulence Models", International Journal of Numerical Methods in Fluids, vol. 28, pp. 601- 616,

Bredberg, J. and Davidson, L. 1999, "Prediction of flow and heat transfer in a stationary two-dimensional rib roughened passage using low-Re turbulent models", paper presented at the Third European Conference on Turbomachinery, IMech C557/074/99, London.

Drain, L.E. and Martin, S. 1985, "Two-component velocity measurements of turbulent flow in a ribbed-wall flow channel", paper presented at the International Conference on Laser Anemometry – Advances and Applications, Manchester, pp. 99-112.

Durao, D.F.G., Gouveia, P.S.T. and Pereira, J.C.F. 1991, "Velocity characteristics of the flow around a square cross section cylinder placed near a channel wall", Expe
riments in Fluids, Vol. 11, pp. 341-50.

Hsieh, K.J. and Lien, F.S., 2005, "Conjugate turbulent forced convection in a channel with an array of ribs", International Journal of Numerical Methods for Heat and Fluid Flow, Vol. 15 No. 5, pp. 462-482

Launder, B.E. and Kato, M. 1993, "Modelling flow-induced oscillations in turbulent flow around a square cylinder", Unsteady Flow, FED-Vol. 157, ASME, pp. 189-99.

Liou, T.M., Hwang, J.J. and Chen, S.H. 1993, "Simulation and measurement turbulent heat transfer in a channel with periodic ribs on one principal", Journal of Heat and Mass Transfer, Vol. 36 No. 2, pp. 507-17.

Nakagawa, S., Senda, M., Hiraide, A. and Kikkawa, S. 1999, "Heat transfer characteristics in a channel flow with a rectangular cylinder", JSME International Journal Series B, Vol. 42, pp. 188-96.

Patankar, S.V. 1980, "Numerical Heat Transfer and Fluid Flow", Hemisphere, Washington, DC.

Tsai, W.B., Lin, W.W. and Chieng, C.C. 2000, "Computation of enhanced turbulent heat transfer in a channel with periodic ribs", International Journal of Numerical Methods for Heat and Fluid Flow, Vol. 10 No. 1, pp. 47-66.

Valencia, A. 2000, "Turbulent flow and heat transfer in a channel with a square bar detached from the wall", Numerical Heat Transfer Part A, Vol. 37, pp. 289-306.

Wang, Y. and Vafai, K. 1999, "Heat transfer and pressure loss characterization in a channel with discrete flush-mounted and protruding heat sources", Experimental Heat Transfer, Vol. 12, pp. 1-16.

Young, T.J. and Vafai, K. 1999, "Experimental and numerical investigation of forced convective characteristics of arrays of channel mounted obstacles", ASME Journal of Heat Transfer, Vol. 121, pp. 34-42.

Young, T.J., Vafai, K., 1998, "Convective flow and heat transfer in channel containing multiple heated obstacles", International. J. Heat Mass Transfer, Vol. 41, pp. 3279–3298.